LASER INTERFEROMETER GRAVITATIONAL WAVE OBSERVATORY
-LIGO-
CALIFORNIA INSTITUTE OF TECHNOLOGY
MASSACHUSETTS INSTITUTE OF TECHNOLOGY

Technical Note **LIGO-T070026- 00- W** 15 April 2007

Status of the LIGO photon calibrators: February 2007

Evan Goetz, Peter Kalmus, Rick Savage

DRAFT

California Institute of Technology
LIGO Project - MS 18-34
Pasadena CA 91125
Phone (626) 395-2129
Fax (626) 304-9834
E-mail: info@ligo.caltech.edu

Massachusetts Institute of Technology
LIGO Project - MS NW17-161
Cambridge, MA 02139
Phone (617) 253-4824
Fax (617) 253-4824
E-mail: info@ligo.mit.edu

WWW: http://www.ligo.caltech.edu/

Contents

1 Introduction

This document describes the measurements we have made using the photon calibrator. We also discuss investigations to understand the differences between using the official method and the photon calibrator to calibrate the end test mass (ETM) coil actuators.

2 Principle of operation

A single photon of frequency ν carries momentum p

$$p = \frac{h\nu}{c} \tag{1}$$

where h is Planck's constant and c is the speed of light. If the photon reflects with angle of incidence θ from the surface of a macroscopic object (such as an ETM), it transfers momentum

$$p_{refl} = 2p\cos\theta \tag{2}$$

to the object where p_{refl} is the transferred momentum. Suppose that there are n such photons per second with energy $h\nu$, then a force $F(t)$ will be produced

$$F(t) = \frac{dp_{refl}}{dt} = \frac{2\cos\theta}{c}\frac{d\left(h\nu n\right)}{dt} = \frac{2\cos\theta}{c}P(t) \tag{3}$$

where $P(t)$ is the power of a stream of photons as a function of time.

During the calibration procedure we want modulate the power to drive the test mass sinusoidally, so the total power may be expressed as a sinusoidal power

$$P(\omega, t) = P_{dc} + P_0 e^{i\omega t}, \tag{4}$$

where ω is the angular frequency of the beam power modulation, P_{dc} is the DC offset and it pushes the test mass with a constant force, and P_0 is amplitude of the power modulation.

If the suspended test mass is treated as a simple pendulum, its equation of motion is given by

$$\frac{F(\omega, t)}{M} = \frac{2\cos\theta}{Mc}P_0 e^{i\omega t} = \ddot{x}(\omega, t) + \gamma\dot{x}(\omega, t) + \omega_0^2 x(\omega, t) \tag{5}$$

where M is the mass of the test mass, γ is the velocity dependent damping coefficient, and $\omega_0^2 = g/l$ is the resonant frequency ($\omega_0 = 2\pi f_0$) with g is the acceleration of gravity and l is the length of the pendulum suspended mass.

The the complex amplitude of the sinusoidal motion ($x(\omega, t) = x_0 e^{i\omega t}$) in response to the sinusoidally modulated force is given by

$$x_0(\omega) = \frac{2P_0\cos\theta}{Mc}\frac{1}{\omega_0^2 - \omega^2 + i\omega\omega_0/Q} \tag{6}$$

where $Q = \omega_0/\gamma$ is the quality factor.

If the frequency of modulation of the beam is much higher than the resonance frequency of the pendulum, $\omega \gg \omega_0$, then this reduces to

$$x_0(\omega) \simeq -\frac{2P_0\cos\theta}{Mc\omega^2}. \tag{7}$$

2.1 Correction due to beam mis-centering

There is a correction due to potentially uncentered main interferometer and photon calibrator beams. If the photon calibrator beam is not centered on the test mass, it will cause an angular motion of the test mass at frequency ω. If the main interferometer beam is perfectly centered there will be no net effect in the gravitational wave channel, to first order in the rotation angle, ϕ. However, if the main beam is not centered, the interferometer will interpret the angular motion as a longitudinal length change.

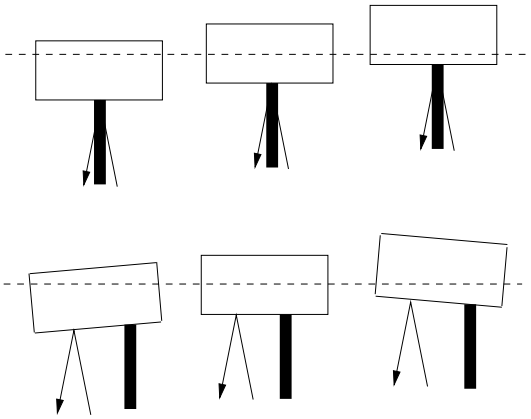

Figure 1: The top images show the ETM motion if both the photon calibrator and interferometer beam are centered. If the photon calibrator and interferometer beams are not aligned, as in the bottom images, then there is an induced rotation which is either in-phase or out of phase with the pendulum motion.

Let us assume, as before, that the frequency modulation of the power is much greater than the pendulum and rotational resonant frequencies of the suspended test mass. Then we could write,

$$M\ddot{x}(\omega,t) = F(\omega,t) \tag{8}$$
$$I\ddot{\phi}(\omega,t) = aF(\omega,t). \tag{9}$$

where I is the rotational inertia of a right circular cylinder about an axis through the center of mass perpendicular to the circular surface, ϕ is the rotation angle, and a is the distance away from the axis of rotation the photon calibrator beam is aligned. Solving these differential equations, we have for the displacement of the center of mass

$$-\omega^2 M x_0(\omega) = \frac{2P_0\cos\theta}{c} \tag{10}$$
$$x_0(\omega) = -\frac{2P_0\cos\theta}{Mc\omega^2} \tag{11}$$

and the angular rotation,

$$-\omega^2 I\phi_0(\omega) = \frac{2P_0 a\cos\theta}{c} \tag{12}$$
$$\phi_0(\omega) = -\frac{2P_0 a\cos\theta}{Ic\omega^2} \tag{13}$$

The rotation of the test mass will be sensed by the interferometer if the interferometer beam is also displaced from the axis of rotation. If the interferometer beam is displaced by a distance b, then the interferometer cavity will lengthen by a factor

$$x_\phi(\omega) = b\sin\phi \simeq b\phi = -\frac{2P_0 ab\cos\theta}{Ic\omega^2} \tag{14}$$

Then the actual displacement due to motion of the center of mass and that due to rotation is

$$x' = x_0 + x_\phi = -\frac{2P_0\cos\theta}{Mc\omega^2}\left(1+\frac{abM}{I}\right). \tag{15}$$

Assuming a well centered photon calibrator beam, or interferometer beam, then with proper knowledge of P_0 and ETM mass M the response of the interferometer can be obtained.

3 Experimental setup

Two photon calibrator units are mounted on each of the three LIGO interferometers, one near each end test mass (Figure 3). The laser of each photon calibrator is aimed at the end test mass reflective surface. Either photon

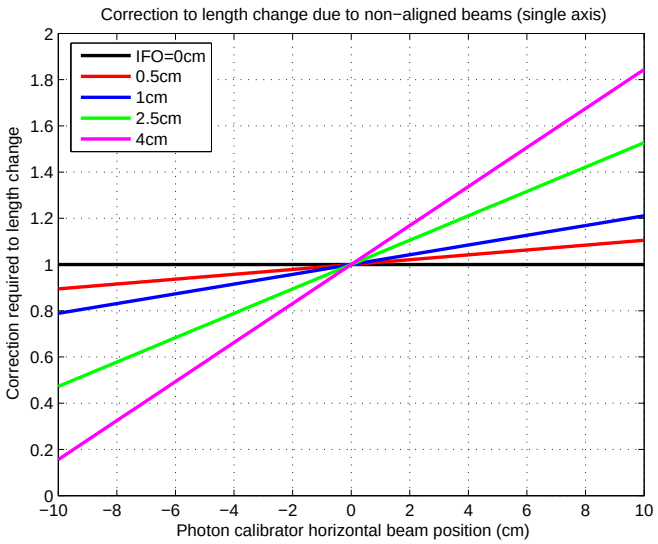

Figure 2: The theoretical prediction of the correction factor $1 + abM/I$ for various interferometer beam offsets as a function of photon calibrator beam offset.

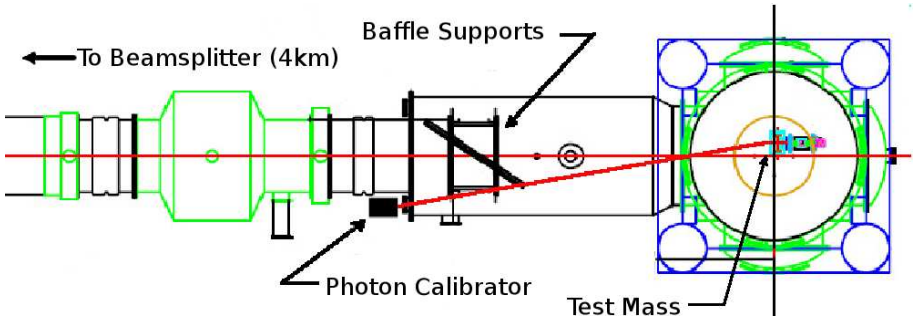

Figure 3: Top view of photon calibrator enclosure mounted near an end test mass. A beam enters the vacuum chamber through a glass viewport and is aimed as close to the center of the test mass as possible to avoid inducing torque on the test mass. In the case of the Hanford 4 km detector (shown here) the beam must pass between two vertical baffle supports and is misaligned from the center of mass.

calibrator can be used to measure the response function of a given interferometer, but one on each end test mass is necessary to reduce the errors when calibrating the coils because differences in the mass of the mirrors will introduce an error unless the mass is well known.

The major components of the system (see Table 1) are a ~ 500 mW 1047 nm Nd:YLF laser; an acousto-optic modulator (AOM) which modulates the laser beam power; and a photodetector which monitors a small fraction ($\sim$1%) of the beam power transmitted by a partially reflecting mirror. Monitoring of the sample beam allows for a calculation of the output power of the system. Once we know the power modulation, we can calculate the expected test mass displacement.

The arbitrary waveform generator (AWG) sends signals to the photon calibrator input through an ICS 110B digital to analog converter. This drives our AOM after passing through filtering electronics. The photodiode within the photon calibrator sends an analog signal (after passing through filtering electronics) to a Pentek analog to digital converter which samples the signal at a data rate of 16384 Hz.

3.1 Photodiode calibration

The calibration of the photodetector within the photon calibrator is very important in obtaining a correct calibration of the interferometer. This calibration factor is proportional to the power reflecting off of the optic, P_{optic},

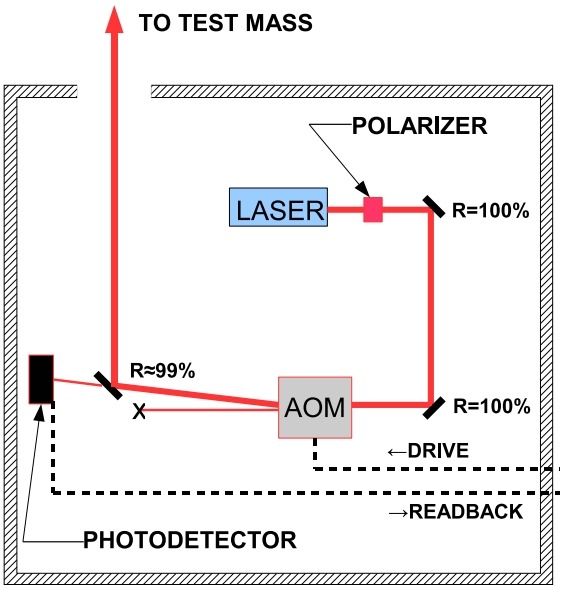

Figure 4: Schematic layout of a photon calibrator optical table showing major components of the system. This optical table is installed inside the enclosure which is mounted as shown in Fig. 3. The beam passes through a polarizer and the AOM before being emitted from the enclosure, through the viewport into the vacuum system and onto the test mass. A small fraction of the beam is continuously picked off for readback by the photodetector, so that power incident onto the test mass can be estimated.

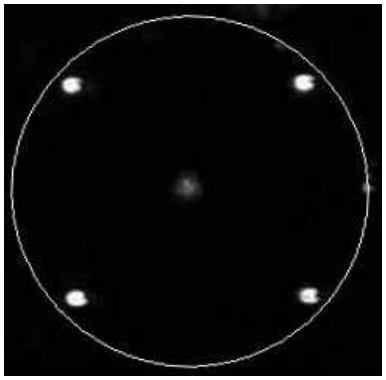

Figure 5: Photo of an end test mass, suspended *in situ*, with a photon calibrator beam visible at the center. The 4 spots near the edge of the test mass mark the locations of the coil actuators. The white circle marks the approximate edge of the test mass. Spacing between adjacent coil actuators is about 16 cm, and test mass diameter is about 25 cm.

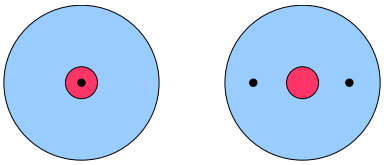

Figure 6: Schematic diagrams of single beam (left) and split beam (right) photon calibrator setups, showing the main interferometer beam in red and the photon calibrator beam(s) in black incident on a test mass.

Table 1: Major components of the system.

Item	Notes	Vendor	Model No.
Laser	500mW 1047nm Nd:YLF	CrystaLaser	IRCL-500-1047
AOM	30MHz bandwidth	Isomet	1205C-843
AOM Driver	80MHz center freq.	Isomet	232A-1
Photodetector	5-mm Ge	New Focus	2033

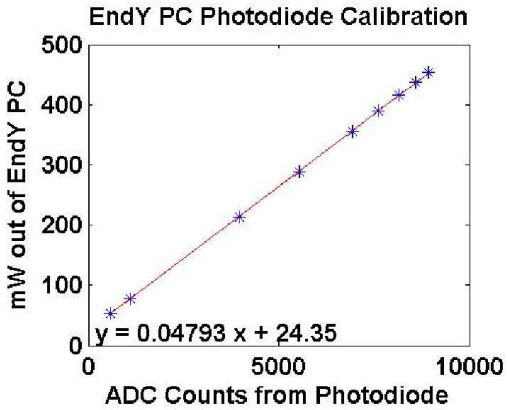

Figure 7: Example photodetector conversion factor (α_c) plot. Only the slope of the line is important, as measurements will always be peak-to-peak.

where

$$P_{optic} = (T_{VP})\,(R_{TM})\,P_{box} \tag{16}$$

where the two multiplicative factors, viewport transmission T_{VP} and test mass reflectivity R_{TM} are slightly less than 1, and it is assumed that there is no other power loss between the enclosure and the optic. P_{box} is the power emerging from the enclosure, and it can be written in terms photodetector readout channel:

$$P_{box} = \alpha_c V_{PD} \tag{17}$$

where V_{PD} is the number of DAQ counts, or volts, returned by the photodetector readout channel, and α_c is a conversion factor in units of power per DAQ counts.

To measure α_c, a handheld power meter was placed in front of the beam immediately before it leaves the enclosure (LHO Ophir unit #4 with thermal head 10A). DAQ counts from the photodetector and the power (in mW) displayed by the power meter were recorded for several different DC voltage values to the AOM driver input. These measurements were made at DC; the transfer function between the input to the AOM driver and the beam power incident on the power meter is reasonably flat from DC up to ~2 kHz (see Section 3.6). We plot the DAQ counts versus power and fit these values to a trendline (Figure 7). The slope of this line is the calibration factor, α_c, of the photodetector.

3.2 Viewport reflection

The viewport reflects a small portion of the incident beam, reducing the total power reaching the ETM. We assume that there is negligable absorption due to the viewport. We measure the incident and reflected power from the viewport. The ratio of these powers gives the reflection coefficient ($R_{VP} = 1 - T_{VP}$). The results for each ETM viewport are given in Table 2.

3.3 ETM reflection

Photons which reflect off of the ETM transfer twice their momentum to the ETM (Section 2). It is necessary to measure the reflection coefficient of the ETMs. This is a difficult measurement and we have tried two methods to measure this.

Table 2: Viewport reflectivities for the six photon calibrator units.

Viewport	Reflectivity [%]	Uncertainty [%]
H1X	7.1	1 or less
H1Y	1.1	negligible
L1X	7.0	1 or less
L1Y	7.7	1 or less
H2X	1.1	negligible
H2Y	0.8	negligible

The first measurement involves using the witness plates of the ETMs in the lab. We measure the reflection coefficient at the working angle of incidence of nine degrees. This incidence angle is the same as that on the interferometers. The results are given below. Here we have assumed that the witness plates have the same reflection properties as the ETMs in the vacuum enclosure of the interferometers.

The second measurement uses the actual ETM in the vacuum enclosure. We aligned a photon calibrator laser beam to reflect off the ETM and exit another viewport by sending the beam in through an optical lever laser viewport (see LHO elog from 10 October 2006 and 22 December 2006). We measured the power into and out of the vacuum enclosure. Then we measured the reflection coefficients of the input and output viewports using the method described in the previous section. These results confirm our lab measurements to within 2 percent. See Appendix C.

3.4 Angle of incidence

To estimate the angle of incidence of the photon calibrator laser beam on the ETMs, we used AutoCad drawings of the location of the photon calibrator in relation to the estimated ETM position in the chambers. For H1 and H2, we estimate the angle of incidence to be 9.7 degrees. We determine this from the geometrical factors in the as-built drawings.

Parameter	**Value**
Transverse horizontal distance	0.96 m
Transverse vertical distance	0.049 m
Longitudinal distance from input surface of Pcal viewport to ETM surface	5.723 m
Transverse distance in plane of incidence	0.96 m
Angle of incidence	9.5 degrees

3.5 ETM mass

Using measurements of the geometry of the ETMs and the density of the test mass substrate, we have estimated the mass of the ETMs from a Matlab script. These calculations were performed on an ITM which was removed from H1. The calculation and measurement of the mass agreed to better than 1 percent. See Appendix E for further details.

Table 3: ETM masses

H1X	**H1Y**	**H2X**	**H2Y**	**L1X**	**L1Y**
10.346 kg	10.388 kg	10.372 kg	10.363 kg	10.353 kg	10.365 kg

3.6 Electronics transfer function

The photodiode calibration is done at DC, but the photon calibrator operates in the range of a few tens of Hz to a few kHz. It is therefore necessary to understand how the calibration is effected at higher frequencies by

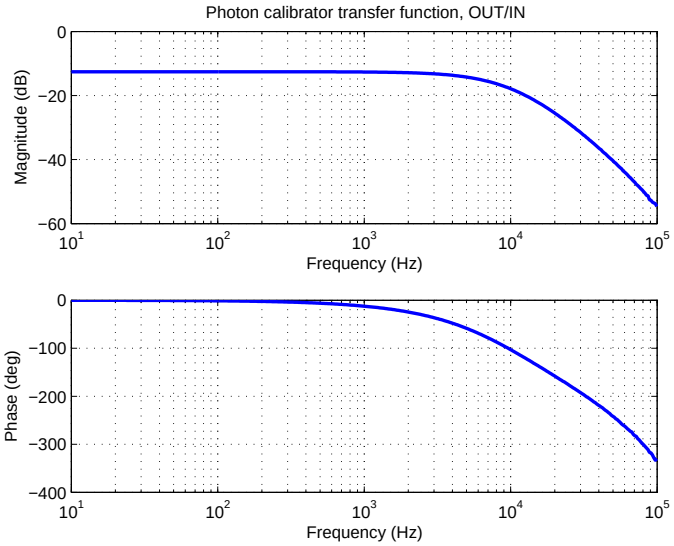

Figure 8: An example transfer function of a photon calibrator. An excitation is sent to the photon calibrator input and the readback to the DAQ is the output.

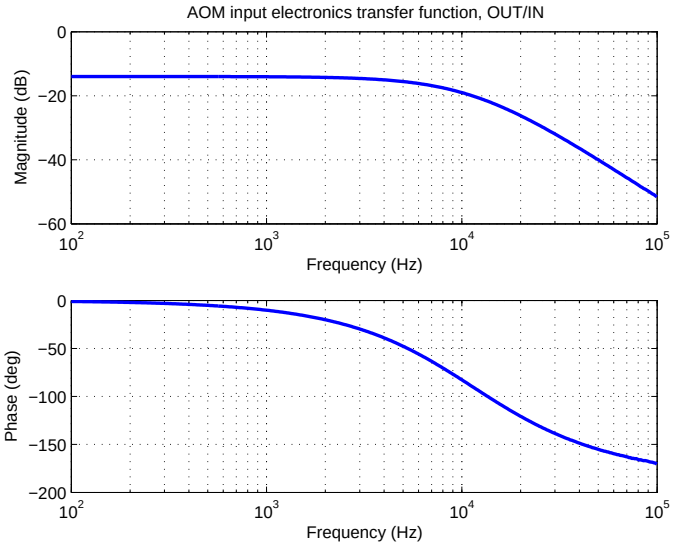

Figure 9: An example transfer function of the input AOM electoronics. An excitation is sent to the photon calibrator input and the signal to the AOM driver input is the output.

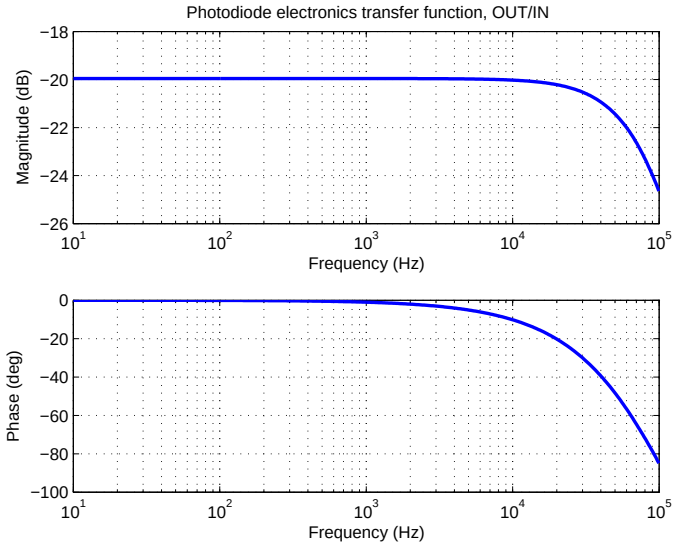

Figure 10: An example transfer function of the output photodiode electoronics. An excitation is sent to the photodiode electronics input and the signal to the DAQ is the output.

measuring the transfer functions of the photon calibrator and associated electronics. Below are the results of the transfer function measurements made between 10 Hz and 100 kHz.

From Figure 8 we have determined that the photon calibrator drive and readback is flat to less than 1 percent at 1.6 kHz, our nominal S5 operating frequencies. The readback alone is flat to less than 1 percent, as shown in Figure 10. At high frequencies (¿2 kHz), the calibration of the photodiode (which is done effectively at DC) must be adjusted for the roll-off of the photodiode electronics.

4 Measurements and results (Need to put in terms of free mass)

4.1 Response function

The response of an interferometer to an external disturbance is determined by the gain of the DARM servo loop and the sensing function of the interferometer. Together these give the response function of the interferometer to an external disturbance.

To measure the response function with the photon calibrator, we inject into ifo:LSC-ETMi_CAL_EXC and read back the two channels ifo:LSC-DARM_ERR and ifo:LSC-ETMi_CAL, the latter being the photodetector read back channel. For an example, see Figure 11. The result of this measurement is then scaled by the expected motion of a free mass (Equation 15). See Figure 13. By scaling the transfer function, we directly measure $R(\omega, t)$.

The loop algebra for using the photon calibrator gives the transfer function,

$$\frac{\text{DARM\_ERR}}{\text{ETMX\_CAL}} = -\frac{\gamma(t)C(\omega,t_0)}{1+\gamma(t)G(\omega,t_0)} b_{\text{X}} \text{pendX} \tag{18}$$

for the X-arm photon calibrator and

$$\frac{\text{DARM\_ERR}}{\text{ETMY\_CAL}} = \frac{\gamma(t)C(\omega,t_0)}{1+\gamma(t)G(\omega,t_0)} b_{\text{Y}} \text{pendY} \tag{19}$$

for the Y-arm photon calibrator. In these transfer function equations, b_{X} and b_{Y} are the calibration of the photon calibrators at DC and pendX and pendY are the pendulum transfer functions normalized to 1 at DC

$$\text{pendi} = \frac{\omega_{\text{i0}}^2}{\omega_{\text{i0}}^2 - \omega^2 + i\omega\omega_{\text{i0}}/Q}. \tag{20}$$

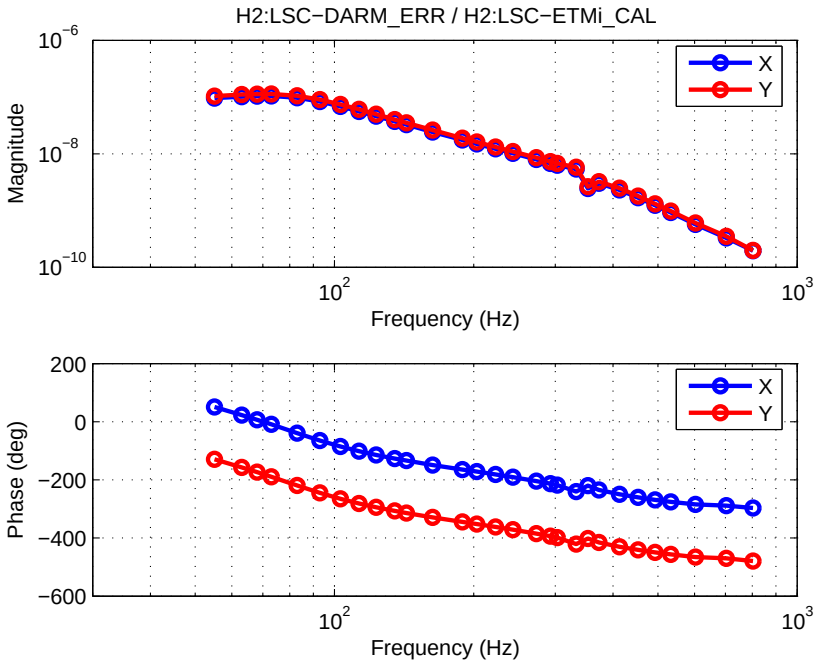

Figure 11: Uncalibrated transfer functions on H2 produced by the photon calibrators on November 8, 2006. The upper plot shows the magnitude (blue is the x-arm and red is the y-arm), the lower plot shows the phase with the x and y arms 180 degrees out of phase.

Similarly, we can also inject into the coil actuators on ifo:LSC-ETMi_EXC, reading back ifo:LSC-DARM_ERR. See Figure 12. This measurement can be scaled once the coils have been calibrated using either the "official" calibration method or using the photon calibrator (see Section 4.2).

Again, the loop algebra for the voice-coil excitation points gives the transfer functions give

$$\frac{\text{DARM\_ERR}}{\text{LSC-ETMX\_EXC}} = -\frac{\gamma(t)C(\omega,t_0)}{1+\gamma(t)G(\omega,t_0)}a_{\text{X}}\text{pendX} \tag{21}$$

for the X-arm voice-coil and

$$\frac{\text{DARM\_ERR}}{\text{LSC-ETMY\_EXC}} = \frac{\gamma(t)C(\omega,t_0)}{1+\gamma(t)G(\omega,t_0)}a_{\text{Y}}\text{pendY} \tag{22}$$

for the Y-arm voice-coil. Here, a_{X} and a_{Y} are the voice-coil calibrations at DC.

4.2 ETM coil calibration

4.2.1 ETM excitations

The photon calibrators inject directly onto the ETM while the voice-coil actuators inject into the actuation path after the output matrix but before the ETM digital actuation filters. Either the photon calibrator or the voice-coil actuators can be used to measure the response function, but the voice- coils must be calibrated prior to their use as a calibrator themselves. Likewise, the photon calibrators are also calibrated prior to use, but in a much simpilar manner.

By taking the ratio of photon calibrator transfer function and voice-coil actuator transfer function measurements taken simultaneously or nearly-simultaneous, we can obtain the coil actuator DC calibration coefficients a_{X} and a_{Y} provided the photon calibrator DC calibration is known:

$$\frac{\text{ETMi\_CAL}}{\text{LSC-ETMi\_EXC}} = \frac{a_{\text{i}}}{b_{\text{i}}}. \tag{23}$$

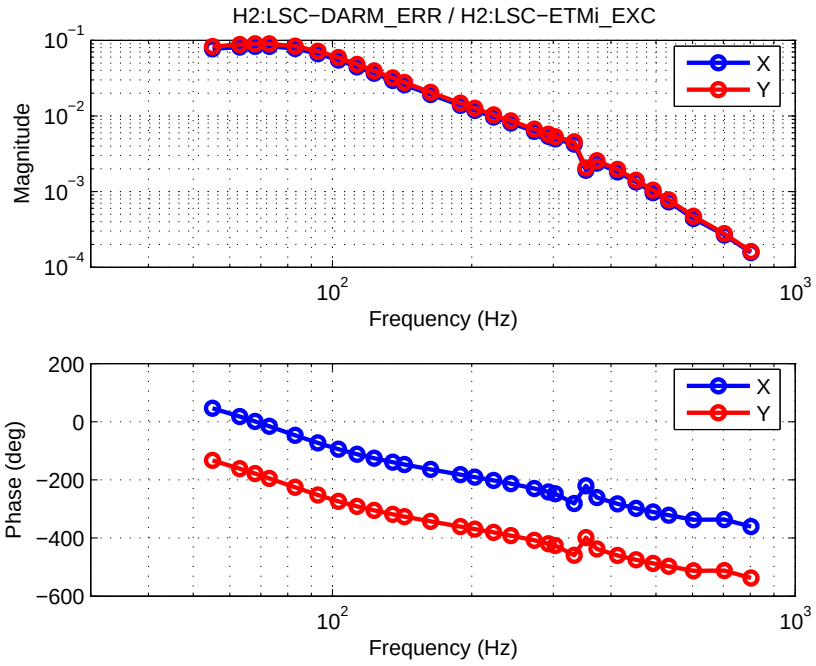

Figure 12: Uncalibrated transfer functions on H2 produced by the coil actuators on November 8, 2006. The upper plot shows the magnitude (blue is the x-arm and red is the y-arm), the lower plot shows the phase with the x and y arms 180 degrees out of phase.

4.2.2 ETM coil calibration results

We can use the photon calibrators to calibrate the ETM voice-coil actuators in terms of meters moved per excitation count. By driving an ETM sinusoidally at a given frequency with a photon calibrator, followed by driving the same ETM with the voice-coil actuators at the same frequency (or driving at the same time, but separated by a small difference in frequency). By taking the ratio of the two transfer functions, the closed-loop gain, pendulum transfer function of the ETM and sensing function of the interferometer divide out. The result is the ratio of the DC gain of each method of excitation.

4.3 Precision and reproducability of the photon calibrator

To understand how reproducable the photon calibrator measurements were, we ran an experiment with the photon calibrator and coils running for 5 hours on H2. The lines were offset from one another by 1.5 Hz all running near 803 Hz. By taking many FFT amplitudes from each of DARM_ERR, ETMi_CAL and ETMi_EXC and taking the appropriate ratios, we can observe the calibration variation as a function of time.

== Need to add the time series and histograms (correlation plots too?) with discussion ==

During the S5 run, we made several measurements on H2 with the photon calibrator. In Figure 17, we plot the DC calibration of the H2 y-arm coil actuator coefficient as produced by the photon calibrator. This covers two different optical configurations of the photon calibrator box. We conclude that a change in the configuration with a new photodiode calibration measurement does not affect the overall result of the photon calibrator.

4.4 Mirror rotation

In 2005, PK made a measurement to observe how an offset in the photon calibrator beam changes the calibration obtained. First, a calibration for how many knob turns of an optical mount it takes for the beam to scan left and right across the ETM. Then, with the interferometer in full lock, a scan was made across the surface with the photon calibrator beam. The approximate beam position is noted and the measurement number is given in Figure 18.

This experiment validates the correction term used in Equation 15 due to off-centered beams.

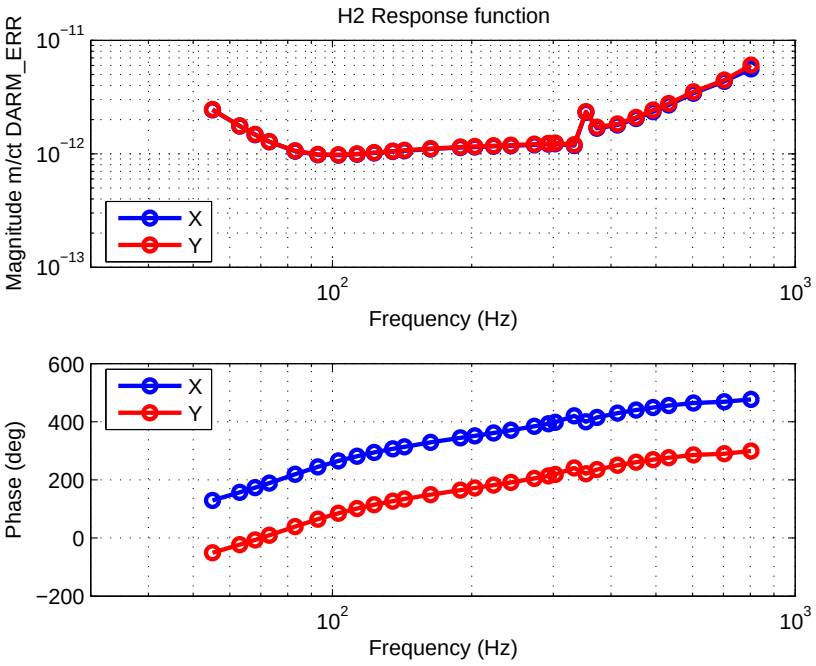

Figure 13: Response function of H2 produced by the photon calibrators. The upper left plot shows the magnitude (blue is the x-arm and red is the y-arm), the lower left plot shows the phase, the upper right shows a ratio of the magnitudes (x-arm/y-arm) and the lower right shows the difference in phase (x-arm minus y-arm).

4.5 Calibration discrepancy

We have therefore performed a measurement of the absolute coil actuation calibration coefficient for an end test mass (ETM) using the photon calibrator. This value can then be compared to conventional measurements. The results are presented in Table 4. The Hanford detectors show agreement between the photon calibrators and the conventional calibration of 16 to 17 percent, while the L1 detector shows agreement between 8 and 14 percent.

Table 4: Summary of photon calibrator discrepancies.

Optic	Pcal ETM Cal	V2 Coil ETM Cal (Free mass at 1 Hz)	Pcal / Coil
H1 ETMX	N/A	0.470×10^{-9} m/ct	N/A
H1 ETMY	0.567×10^{-9} m/ct	0.489×10^{-9} m/ct	1.16
H2 ETMX	0.559×10^{-9} m/ct	0.482×10^{-9} m/ct	1.16
H2 ETMY	0.612×10^{-9} m/ct	0.523×10^{-9} m/ct	1.17
L1 ETMX	0.291×10^{-9} m/ct	0.255×10^{-9} m/ct	1.14
L1 ETMY	0.258×10^{-9} m/ct	0.239×10^{-9} m/ct	1.08

5 Uncertainty (Need Peter's recommended fixes)

In this section we estimate the uncertainty inherent in the estimation of test mass displacement with photon actuators. This uncertainty will factor into the uncertainty of any detector calibration made with the device.

The following quantities must be measured in order to estimate a test mass displacement due to radiation pressure via equation 15:

1. Power reflecting off of the test mass, obtained by measuring

    1. the sampling photodetector response;

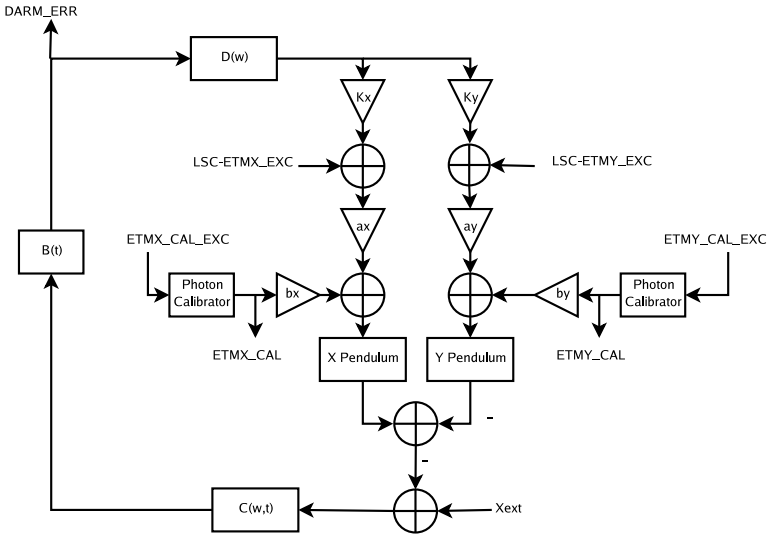

Figure 14: A schmatic of the DARM servo loop with details identifying the injection points in the loop.

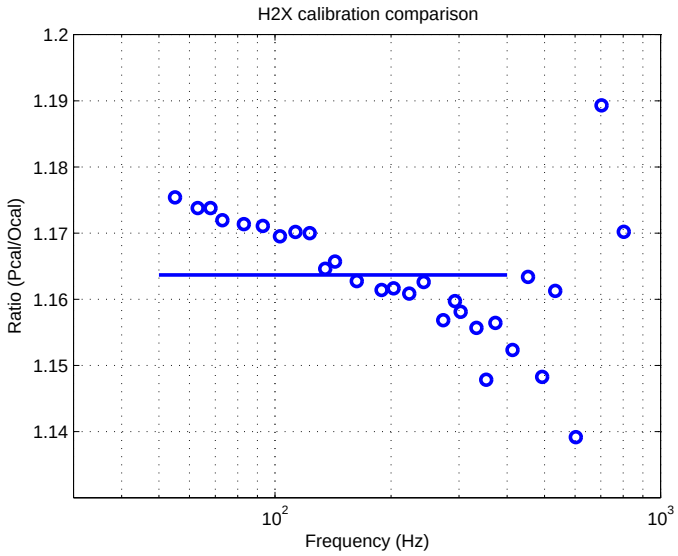

Figure 15: H2 ETMX voice-coil calibration propagated to DC produced from the photon calibrators compared to the V2 calibration value.

2. the photodetector calibration factor;
3. the transmission of the viewport;
4. and transmission of power through the test mass;

2. angle of incidence of the beam to the test mass;

3. mass of the test mass;

4. photon calibrator and main interferometer beam offsets from the center of the test mass.

Our goal in this section is to estimate uncertainties on each of these measurements, and then to combine them into an uncertainty on the test mass displacement.

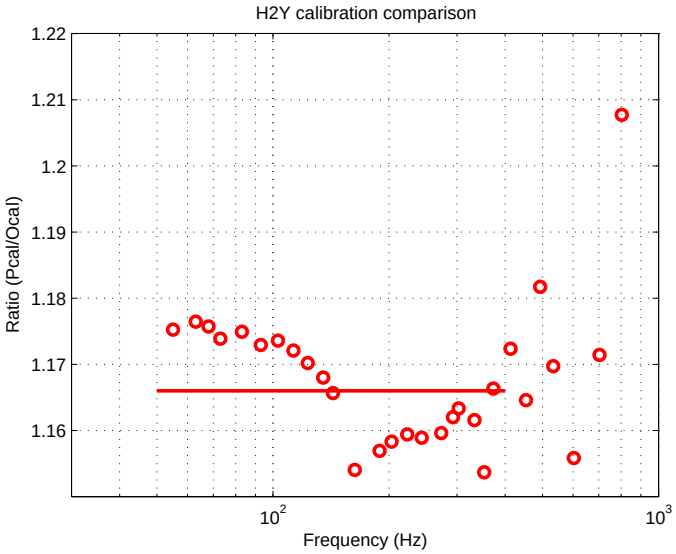

Figure 16: H2 ETMY voice-coil calibration propagated to DC produced from the photon calibrators compared to the V2 calibration value.

5.1 Sampling photodetector response

We assume that the uncertainty in output from the photodetector, P_{PD}, is negligible compared to other sources at low photon calibrator frequencies. We use P_{PD} to determine a calibrated power, so only non-linearities across amplitude or a non-flat frequency response could contribute to error. Frequency roll off in the transfer function between the AOM input is about 0.15% at 803 Hz, and even less at lower frequencies.

It would be nice to try the following experiment to verify this assumption:

1. at 100 Hz, measure a comb of amplitudes put in with the AOM and make sure it's linear to less than a percent across the range we use.

5.2 Photodetector Calibration Factor

Error in the photodetector calibration factor α_c could arise from non-stationarity in both the photodetector and the power meter used to make to calibrate the device, and in the absolute calibration of the power meter, in addition to measurement error.

Uncertainty from non-stationarity and measurement error could be estimated by calculating the standard deviation of N α_c measurements made over a long period of time (assuming the measurements are Gaussian distributed). Since the measurement is not made often, N is small and we must use Student's t-distribution to account for the poor parameter estimation. Uncertainty estimated in this way is less than 10% for all photon calibrators (Table 5, and would likely be less than 3% if in all cases only one power meter were used and it were not recalibrated over the course of the series of measurements.

There is an additional uncertainty due to the absolute calibration of the power meter used in the measurement. The 1σ uncertainty in measurements made with 6 similar power meters was found to be 1.7%. We add this in quadrature to the uncertainty in measurements of α_c already described.

Measuring α_c turns out to be the dominant source of uncertainty at low frequencies ($\lesssim 800$ Hz).

5.3 Viewport reflectivities

Uncertainty in the viewport transmission factor contributes to the uncertainty in the power incident on the test mass, and therefore to the uncertainty in the test mass displacement(equation 16). The quantity measured is fraction of power reflected by the viewport.

Measurements were made with an Ophir PD300 head, which has a nominal uncertainty of $\sim$1% in ideal conditions (e.g. beam size much smaller than sensor size). Measuring reflectivity requires measuring incident

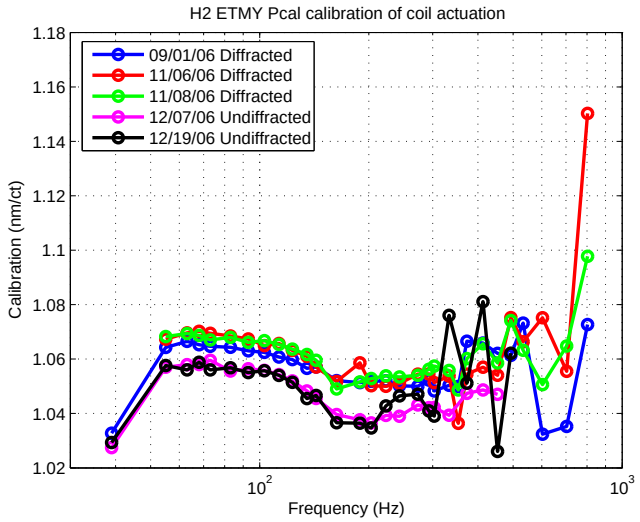

Figure 17: Several measurements made with the photon calibrators over a three month period on the H2 interferometer showing agreement to better than 2% up to $\sim$400 Hz.

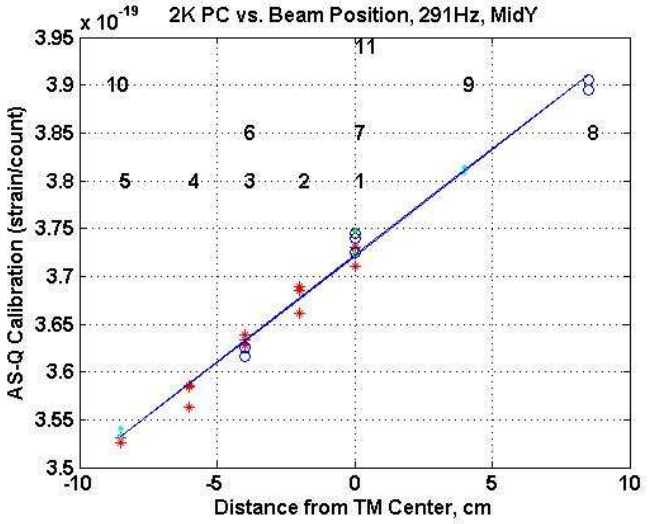

Figure 18: Experimental verification of the correction term in equation 15 due to off-centered beams. The x-axis shows approximate position of the photon calibrator beam relative to the center of the test mass, and the y-axis shows the magnitude of the response function $R(\omega)$. The fit to experimental data indicates that the main interferometer beam was offset by 2.8 mm to left of center. The measurements were made on the Y-arm of the H2 interferometer.

Table 5: Photodetector conversion factor (α_c) measurements [mW/(ADC counts)]. The Livingston Observatory's numbers (L1) differ from Hanford's (H1 and H2) probably because Livingston uses different photodetector pickoff mirrors. The 'X' and 'Y' in the unit names refer to the two arms of each interferometer, the 'X-arm' and 'Y-arm.' All measurements were made with the same power meter except for the 05/10/10 measurements. This power meter was recalibrated after the 06/6 measurements. Finally, some measurements were made in one-beam configuration, while others were made in the two-beam configuration. The percentage uncertainties, calculated with Student's t-distribution, do not account for power meter recalibration, different power meters, or different beam configurations, and thus represent worst-case estimates.

Unit	05/7/27	05/8/12	05/8/16	05/9/22	05/10/10	06/6	06/11	06/12	$\frac{\sigma}{mean}$ [%]
H1X	–	0.0450	0.0444	0.0462	–	0.0438	–	–	2.7
H1Y	0.0480	0.0479	–	0.0471	–	0.0459	–	–	2.5
L1X	–	–	–	–	0.0882	–	0.0816	–	10.0
L1Y	–	–	–	–	0.1187	–	0.1138	–	5.4
H2X	–	0.0487	0.0486	0.0496	–	0.0482	0.0445	0.0442	5.4
H2Y	–	0.0504	–	0.0505	–	–	0.0490	–	2.2

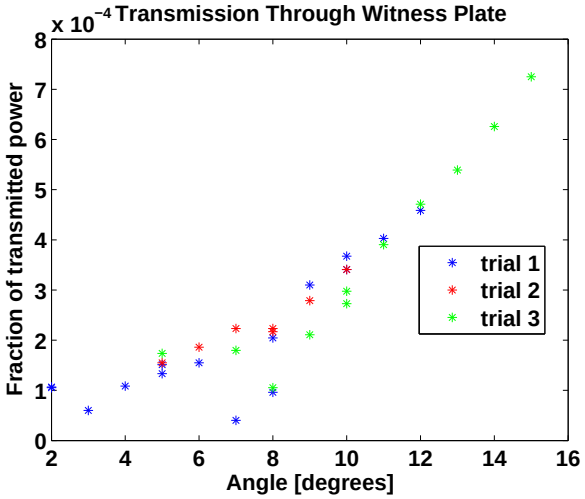

Figure 19: Transmission fraction through an end test mass witness plate as a function of beam incident angle.

power (a large quantity) and reflected power (a small quantity) with the same head. Assuming that all reflected light is captured, and assuming that the uncertainty in a measurement is constant over the PD300 head's entire dynamic range, the reflectivity ratio would have an uncertainty of $\sim 2\%$. However, since the measurement was difficult to make and the beam size was of the same order as the sensor, we conservatively estimate an uncertainty in reflectivity of $\sim$10%.

A 10% uncertainty on a reflectivity measurement of 0.01 (see Table 2) corresponds to an uncertainty in the transmitted power of 0.1%; thus, reflectivity measurements of the three $\sim 1\%$ viewports contribute negligibly to the overall uncertainty. A 10% uncertainty on a measurement of 0.07 gives (rounding up) a 1% contribution to the overall uncertainty in the calibration factor.

5.4 Transmission through the optic

There is a small adjustment due to transmission of part of the photon calibrator beam through the optic ($1-R_{TM}$ in equation 16).

To determine the factor and its uncertainty, we measured transmitted power through an end test mass witness plate as a function of incident angle, using the H2X photon calibrator in the optics lab.

The witness plate was mounted on a rotating stand. A plot of the fraction of transmitted power as a function of angle of incidence is shown in Fig. 19.

The trend appears to be roughly linear over this range of incident angles. The photon calibrators are mounted on the opposite side of the beam tube from their respective test masses (see Section 5.6), making the nominal

angle of incidence 9.1 degrees and the fraction of transmitted power about 0.03%.

These transmission measurements are not very precise and their uncertainty is relatively large. However, since the fraction of reflected power is very close to 1, uncertainty in the adjustment factor is negligible.

5.5 Mass of the optic

Determination of the mass of the optics has uncertainty of $< 0.1\%$ which is not significant compared to other component uncertainties.

5.6 Beam Angle of Incidence

The test mass displacement is directly proportional to the cosine of the angle of incidence of the beam on the test mass. Uncertainties on this value are less than a tenth of a percent, and we conclude that uncertainty from this source is negligible.

5.7 Off-centered beams

The calibration result depends on the offset from center of both the main interferometer beam (b) and the photon calibrator beam (a) according to equation 15. We wish to determine uncertainty in the quantity

$$\alpha_{beam} = 1 + \frac{abM}{I}, \tag{24}$$

which is a multiplicative factor in equation 15.

We again assume that uncertainty in M is negligible compared to uncertainty in the other quantities.

The moment of inertia around the yaw axis I was calculated by assuming the optic is a perfect cylinder, and subtracting values for edge chamfers and a wedge of removed material from the rear face. This calculation should be good to at least 1%, which makes uncertainty in I negligible compared to uncertainties in a and b, discussed below.

Typically b tends to wander and is not known precisely at any given time; it can be determined precisely by sweeping the photon calibrator beam across the optic as in figure 18, but it would not be practical to perform this measurement before every photon calibrator measurement.

We thus estimate a range of values for b which will include the actual value at least 68% of the time, and use the boundaries of this range in conjunction with uncertainty on a and I to estimate uncertainties on α_{beam}. We assume b to be less than 4 mm at least 68% of the time, and we conservatively estimate an uncertainty on a of 3 mm.

If a is nominally zero, these considerations give an uncertainty on α_{beam} of less than 0.5%, which is an insignificant uncertainty.

However, a is not always nominally zero. Supports for beam tube baffles are in place at the two Hanford end stations, and they obstruct the path of the H1 photon calibrator beams onto the centers of the test masses. It is therefore necessary to place these beams approximately 2 cm from the center of the test mass. Supports have not yet been installed at the Hanford mid stations or at Livingston; H2 and L1 photon calibrator beams are centered.

An investigation using H2 was made to see what effect beam off-centering has on the calibration factor. At the time of this investigation the main beam was offset by 2.8 mm. It was found that under these conditions a 2 cm offset corresponds to a $\sim 1.3\%$ perturbation in the calibration factor, or $\alpha_{beam} \sim 0.987$. However, if the value of b were to change, this value of α_{beam} could vary between ~ 0.98 and ~ 1.00 for our stated range of b and uncertainty in a.

Therefore we propose a conservative uncertainty in α_{beam} for off-centered photon calibrator beams to be $\sim$2% if b is not measured.

If it is not convenient to alter the baffle design for the photon calibrators, it would be possible to reduce this uncertainty in the calibration factor if b could be measured.

5.8 Combined uncertainty in test mass displacement

Uncertainties in the test mass displacement estimate are summarized in Table 6. Since each component uncertainty is for a measured quantity which enters as a factor in equation 16, relative uncertainties from independent sources can be added in quadrature to estimate total uncertainty.

Table 6: Significant 1σ component uncertainties in test mass displacement estimates, and combined uncertainty [%] of the six photon calibrator units. Component uncertainties added in quadrature to arrive at the combined uncertainty.

	H1X	H1Y	L1X	L1Y	H2X	H2Y
Photodetector Calibration	2.7	2.5	10.0	5.4	5.4	2.2
Power Meter Calibration	1.7	1.7	1.7	1.7	1.7	1.7
Viewport Transmission	1.0	-	1.0	1.0	-	-
Off-centered Beam	2.0	2.0	-	-	-	-
Overall	3.9	3.6	10.2	5.7	5.7	2.8

5.9 Uncertainty in detector calibration

Measurement of detector calibration involve measurement of test mass displacement and measurement of response in the gravitational wave channel of the detector. In the case of calibration performed at low photon calibrator frequencies with sufficient integration time, uncertainty in the measurement of detector response is negligible. Thus the intrinsic uncertainty in a calibration is the uncertainty due to estimating the test mass displacement. Of course, at high frequencies or in the case of insufficient measurement time the uncertainty in a detector calibration will increase.

6 Conclusion

Photon calibrators provide an independent calibration of LIGO's three gravitational wave detectors. Agreement with the conventional calibration is at the 15-20% level for the two Hanford detectors, and at the $\sim$5% level at Livingston. Intrinsic ncertainty in these results at the 1σ level is between 3% and 10% for the six LIGO photon calibrator units. Since the uncertainty on the conventional calibration is estimated to be $\sim$5%, there is an unresolved systematic discrepancy at the two Hanford detectors. In the future, we hope to resolve the discrepancy.

Finally, we note that the photon calibrators have the potential for measuring phase lags in the detectors' control systems, and for injecting calibrated hardware waveforms into gravitational wave data. Photon calibrator hardware injections could be useful in realistic blind data analysis tests.

Acknowledgements

We are indebted to many of our colleagues for frequent and fruitful discussion. In particular we would like to thank David Barker, GariLynn Billingsley, Douglas Cook, Mark Guenther, and Richard McCarthy for valuable suggestions and support.

The authors are grateful for the support of the United States National Science Foundation under cooperative agreement PHY-04-57528 and Columbia University in the City of New York. We are grateful to the LIGO collaboration for their support.

The LIGO Observatories were constructed by the California Institute of Technology and Massachusetts Institute of Technology with funding from the National Science Foundation under cooperative agreement PHY-9210038. The LIGO Laboratory operates under cooperative agreement PHY-0107417.

References

A Photodetector calibration

B Viewport reflection

EG and RS observed two spots when the angle of incidence was increased from the nominal 9 degrees angle of incidence (see LHO elog 22 December 2006, following section). In each spot (at higher than normal angle of incidence) the reflection coefficient was 4.4 percent. The viewport used for this measurement was the output viewport of the H2 ETMX optical lever laser. However, it has similar reflection properties as the 7 percent reflecting viewports for the photon calibrators.

C ETM reflection

EG and RS measured the ETM reflectivity in situ using a photon calibrator aimed through an optical lever laser viewport (see LHO elog from 10 October 2006 and 22 December 2006).

```
Today, we utilized the spare photon calibrator laser (1047 nm) to
measure the optical lever output window reflectivity.

Here are the numbers:
Today's measurements (using Ophir power meter #4, solid state
detector without the filter)-
incident power = 8.85 mW
reflected power = 0.502 mW
reflectivity = .502/8.52 -> 7.4%

Earlier measurements:

Power to input viewport (trial 1): 392 mW
Power out of the output viewport (trial 1): 345 mW
(overall efficiency = 345/392 -> 88.0%)

Power to input viewport (trial 2): 387 mW
Power out of the output viewport (trial 2): 342 mW
(overall efficiency = 342/387 -> 88.4%)

Power reflecting off the input viewport: 27.0 mW
reflectivity = 27/((387+392)/2) -> 6.9%

We expect the test mass reflectivity to be 99.97%

Thus we would expect the transmission efficienty to be:

0.931 * 0.9997 * 0.926 = 86.2%

We measured closer to 88%. This is likely due to measuring the output
window reflectivity at closer to normal incidence than during the overall
transmission measurement. Today, we purposely increased the incidence
angle to about 11 deg. so that we could see two distinct reflected spots.
At this angle, the viewport reflectivity was 0.391/8.85 -> 4.4%. The
incidence angle for the photon calibrators is about 9.1 deg. Using the 11
deg. reflectivity, the expected overal transmission would be
0.931 * 0.9997 * 0.956 = 89.0%

Bottom line - there is no anomalous loss of power in the photon
calibrator propagation, at least for MidX.
```

D Angle of incidence

DCC drawing numbers?

Table 7: Parameters to calculate the angle of incidence of the photon calibrator laser beam

Parameter	Value
Transverse horizontal distance to ETM	0.911 m
Transverse vertical distance to ETM	0.100 m
Longitudinal distance to ETM	5.723 m
Transverse offset in plane of incidence	0.916 m
Angle of incidence	9.1 Deg.

E ETM mass

```
% From a Gari e-mail:
%
% Finally... SPETM01
% Diameter 249.848 mm
% Thickness 99.126 to max sharp corner\
% Wedge  1.968 Degrees
% Side one chamfer 1.78 mm
% Side two chamfer 1.98 mm

% from coc as built
% BLANKS
% ETM01  25.677 x 10.901
% ETM02  25.684 x 10.889
%
% SPETM03  25.684 x 10.901
% SPETM05  25.671 x 10.896
% SPETM06  25.054 x 9.995
% SPETM07  25.027 x 10.002

% POLISHED SUBSTRATES
% ETM01  25.075 x 9.963
% ETM02  25.088 x 9.993
%
% SPETM03  25.061 x 9.9863
% SPETM05  25.0482 x 9.9977
% SPETM06  25.054 x 9.995
% SPETM07  25.027 x 10.002

dens = 2.201;                %Suprasil family (we have 312)
% L = 10;                    %test mass cylinder length in cm
% r = 12.5;                  %test mass radius
%
%
% L = 9.9126
% r = 24.9849/2
%
% % L = 10.901
% % r = 25.677/2
%
% ang = 2.0;                 %test mass wedge in deg
```

```
% tmChamferLeg = 0.2;         %test mass chamfer leg length, cm
%
%
% mnom = pi*r2*L*dens         %nominal mass not considering chamfer
%
% angrad = ang/180*pi;                    %test mass wedge in radians
% delm = pi*(12.52)*(sin(angrad)*25)/2   %mass of removed wedge material
% mcham = 2e-2 * pi *25 * dens * 2       %mass of removed chamfers - 2 mm both faces
% m = mnom - delm - mcham                %net mass of test mass in grams




%test mass chamfer leg length, cm, rounded to same value for all ETMs


% POLISHED SUBSTRATES
% ETM01 || 10.346 || 25.075  ||  9.963  || 2d00m  || 0.216 || 0.193 ||
% ETM02 || 10.388 || 25.088  ||  9.993  || 2d00m  || 0.217 || 0.226 ||
%
% SPETM03 || 10.363 || 25.061  ||  9.9863 || 1.989d || 0.212 || 0.180 ||
% SPETM05 || 10.365 || 25.0482 ||  9.9977 || 1.983d || 0.199 || 0.189 ||
% SPETM06 || 10.372 || 25.054  ||  9.995  || 1d58m  || 0.198 || 0.203 ||
% SPETM07 || 10.353 || 25.027  || 10.002  || 1d59m  || 0.193 || 0.211 ||

% results from running this script
% M =
%   10.34569803251292
% M =
%   10.38758907443100
% M =
%   10.36289016520503
% M =
%   10.36508409558616
% M =
%   10.37171099757591
% M =
%   10.35337876052679


dVect = [ 25.075 , 25.088 , 25.061 , 25.0482 , 25.054 , 25.027 ];
lVect = [ 9.963 , 9.993 , 9.9863 , 9.9977 , 9.995 , 10.002 ];
angVect = [ 2, 2, 1.989, 1.989, 1 + 58/60, 1+59/60 ];
chmf1Vect = [ 0.216 , 0.217 , 0.212 , 0.199 , 0.198 , 0.193 ];
chmf2Vect = [  0.193 ,  0.226 , 0.180 , 0.189 , 0.203 , 0.211    ];


% Finally... SPETM01
% Diameter 249.848 mm
% Thickness 99.126 to max sharp corner\
% Wedge  1.968 Degrees
% Side one chamfer 1.78 mm
% Side two chamfer 1.98 mm

%%%%%%%%%%%%%%%%%%%%%%%%%%%%%%%%%%%%%%%%%%%%%%%%%%%%%%%%%%%%%%%%%%%%%%%
```

```
%calculation of mass of ITMx
%expected uncertainty contribution ~1%
%
dens = 2.201;

mVect = [];
for i = 1 : 6

tmLength = lVect(i);
tmRadius = dVect(i)/2;
tmWedgeAngle = angVect(i);
tmChamferLeg1 = chmf1Vect(i);
tmChamferLeg2 = chmf2Vect(i);


% tmLength = 9.963
% tmRadius = 25.075/2
% tmWedgeAngle = 2
% tmChamferLeg = 0.2;

% tmLength = 10
% tmRadius = 25/2

% tmLength = 9.9126
% tmRadius = 24.9848/2

angrad = tmWedgeAngle/180*pi;
%nominal mass not considering chamfer
mnom = pi * tmRadius2 * tmLength * dens;
%mass of removed wedge material
delm = pi * tmRadius2 * (tan(angrad) * 2 * tmRadius) / 2 * dens;
%mass of removed chamfers
mcham1 = (tmChamferLeg12 / 2) * pi * 2 * tmRadius * dens;
mcham2 = (tmChamferLeg22 / 2) * pi * 2 * tmRadius * dens;
%net mass, g
m = mnom - delm - mcham1 - mcham2;
%net mass, kg
M = m/1000

mVect = [mVect M];

end

mean(mVect)
std(mVect)



% tmLength = 9.963
% tmRadius = 25.075/2
% tmWedgeAngle = 2
% tmChamferLeg = 0.2;

% tmLength = 10
% tmRadius = 25/2
```

```
% tmLength = 9.9126
% tmRadius = 24.9848/2

tmLength = 10.901
tmRadius = 25.677/2

angrad = tmWedgeAngle/180*pi;
%nominal mass not considering chamfer
mnom = pi * tmRadius2 * tmLength * dens;
%mass of removed wedge material
delm = pi * tmRadius2 * (tan(angrad) * 2 * tmRadius) / 2 * dens;
%mass of removed chamfers
mcham1 = (tmChamferLeg12 / 2) * pi * 2 * tmRadius * dens;
mcham2 = (tmChamferLeg22 / 2) * pi * 2 * tmRadius * dens;
%net mass, g
m = mnom - delm - mcham1 - mcham2;
%net mass, kg
M = m/1000

mVect = [mVect M];
```